

# Intercalant-independent transition temperature in superconducting black phosphorus

Renyan Zhang<sup>1</sup>, John Waters<sup>2</sup>, Andre K. Geim<sup>1</sup>, Irina V. Grigorieva<sup>1</sup>

<sup>1</sup>School of Physics and Astronomy, University of Manchester, Oxford Road, Manchester M13 9PL, United Kingdom

<sup>2</sup>School of Earth, Atmospheric, and Environmental Sciences, University of Manchester, Oxford Road, Manchester M13 9PL, United Kingdom

Research on black phosphorus (BP) has been experiencing a renaissance over the last few years, after the demonstration that few-layer BP exhibits high carrier mobility and a thickness-dependent band gap<sup>1,2,3,4,5</sup>. For a long time<sup>6,7</sup>, bulk BP is also known to be a superconductor under high pressure exceeding 10 GPa. The superconductivity is due to a structural transformation into another allotrope of phosphorous<sup>6,8</sup> and accompanied by a semiconductor-metal transition<sup>6</sup>. No superconductivity could be achieved for BP itself (that is, in its normal orthorhombic form) despite several attempts reported in the literature<sup>9,10,11,12</sup>. Here we describe successful intercalation of BP by several alkali metals (Li, K, Rb, Cs) and alkali-earth Ca. All the intercalated compounds are found to be superconducting, exhibiting the same (within our experimental accuracy) critical temperature of  $3.8 \pm 0.1$  K and practically identical characteristics in the superconducting state. Such universal superconductivity, independent of the chemical composition, is highly unusual. We attribute it to intrinsic superconductivity of heavily-doped individual phosphorene layers, while the intercalated layers of metal atoms mostly play a role of charge reservoirs.

Bulk BP is the most thermodynamically stable phosphorus allotrope<sup>13</sup> with a moderate direct bandgap (0.3 eV for bulk BP<sup>14</sup>, increasing to 2 eV for monolayer phosphorene<sup>2</sup>). Recent demonstrations of high mobilities<sup>3,5</sup>, quantum oscillations<sup>4</sup>, thickness-dependent gap<sup>5</sup> and field-effect transistors with high on-off ratios<sup>15</sup> using few-layer BP has led to a strong wave of interest in this material in its quasi-two-dimensional form. Furthermore, the band gap of few-layer BP has been predicted to be tuneable by strain<sup>16</sup> and electric field<sup>17</sup>, whereas surface doping of few-layer BP with potassium was found to result in a metallic state<sup>18</sup>. While the interest in semiconducting BP is focused on its promise for nanoelectronics and nanophotonics<sup>1</sup>, metallic BP was predicted to have sufficient electron-phonon coupling to become a superconductor<sup>19,20</sup>.

Metallic state and superconductivity in phosphorous were previously achieved in the 1960s (ref.<sup>6,7</sup>) by applying high pressure. The transition to the metallic state was shown to be associated with the structural transition from the orthorhombic to simple-cubic crystal lattice, which actually means that the latter material was no longer BP but somewhat closer to white phosphorous that also has a cubic lattice<sup>8</sup>. The superconducting transition was found at 4.8 K at 10 GPa and the transition temperature,  $T_c$ , could be further increased to 9.5 K at 30 GPa (refs.<sup>6,7</sup>). The question whether it is possible to induce superconductivity in BP by other means has remained open. Recent experiments on electrostatically-doped thin flakes of BP (ref.<sup>21</sup>) did not find superconductivity, despite being able to

achieve carrier concentrations well above  $10^{13} \text{ cm}^{-2}$ , sufficient to induce superconductivity in, e.g., electrostatically-doped  $\text{MoS}_2$  (ref.<sup>22</sup>). There were also several attempts to obtain intercalated compounds of BP by reacting it with alkali metals<sup>9</sup> (K, Cs and Li), iodine<sup>10</sup>, and  $\text{AsF}_5$  (ref. <sup>11</sup>) and by electrochemical lithiation<sup>12</sup>. No stable intercalation compounds could be achieved in either of these studies, and no superconducting response was reported or discussed.

To overcome the problem of disintegration of BP crystals when in contact with highly reactive vapours of alkali metals, we have employed an alternative technique of liquid ammonia intercalation<sup>23,24</sup>. This allowed us to achieve successful intercalation of BP crystals with several alkali and alkali-earth metals: lithium (Li), potassium (K), rubidium (Rb), caesium (Cs) and calcium (Ca). All our intercalation compounds show superconductivity with  $T_c$  of 3.8 K, the same value within our experimental accuracy of  $\pm 0.1$  K. We emphasise that  $T_c$  does not depend on the intercalating metal, which indicates that the superconductivity is an intrinsic property of electron-doped phosphorene (individual layers of black phosphorus), as described below.

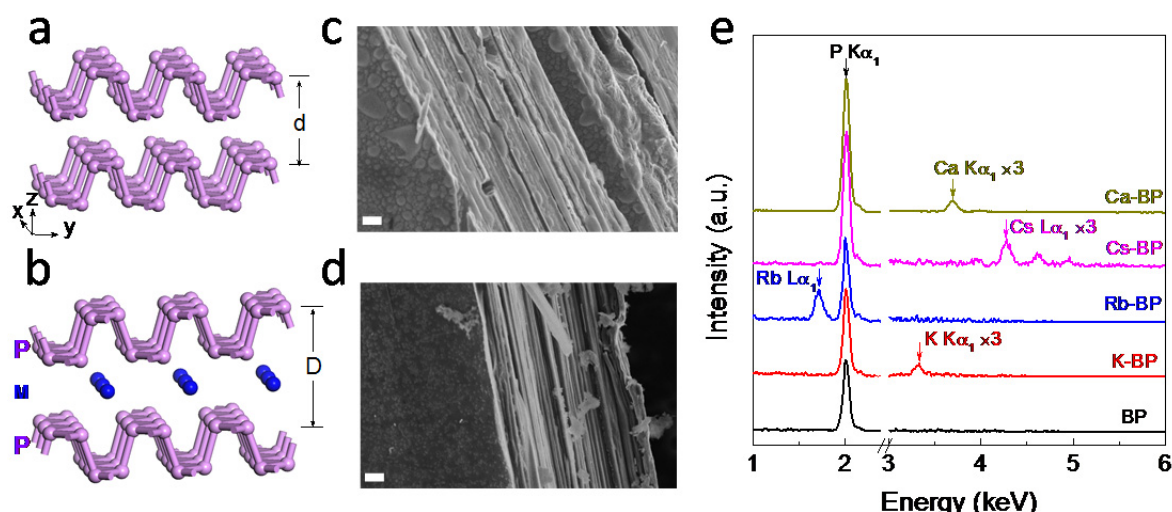


**Figure 1| Structure and composition of pristine and intercalated black phosphorus.** (a, b) Schematic structure of black phosphorus before (a) and after (b) intercalation. ‘P’ stands for phosphorus atoms and ‘M’ represents intercalating metals Li, K, Rb, Cs or Ca. The shown positions of metal atoms correspond to the results of first-principle calculations<sup>20,25,26</sup>. Those suggested that the adjacent phosphorene layers should slide with respect to each other, effectively changing the stacking order of phosphorene layers and providing a maximum space for the metal ions. (c, d) Cross-sectional scanning electron microscopy images of pristine (c) and Cs-intercalated (d) BP. Scale bars, 1  $\mu\text{m}$ . (e) Typical EDS spectra for pristine and intercalated BP.

The atomic arrangements expected for pristine and intercalated BP are shown schematically in Fig. 1a,b (refs.<sup>20,25,26,27</sup>). BP consists of weakly-bonded phosphorene layers, within which covalently bonded P atoms form a honeycomb network, similar to graphene, but each layer is puckered with a zigzag-shaped edge along the x axis and an armchair-shaped edge along the y axis<sup>27</sup>. To achieve metal intercalation and obtain intercalated compounds  $\text{M}_x\text{P}$  (here M stands for Li, K, Rb, Cs and Ca), crystals of black phosphorus were immersed in a metal-liquid ammonia solution at a temperature of  $-78^\circ\text{C}$  in a dry ice/isopropanol (IPA) bath (see Methods for details). The starting solution has a characteristic deep blue colour due to dissociation of metal atoms into solvated cations ( $\text{M}^+$ ) and solvated electrons ( $\text{e}^-$ ), ref. <sup>28</sup>. As intercalation proceeds, the solution gradually loses its colour, which

is known to be an indication of metal ions moving into the van der Waals gaps between the layers of host crystals<sup>23</sup>. This allowed us to monitor the process visually. Intercalation was also apparent from significant swelling of the crystals, with an expansion along the z axis (for example, a sample with thickness of 0.4 mm expanded to 1.0 mm). The intercalation process started at the surface of the host crystal and, as described below (see also ref. <sup>23</sup>), resulted in a superconducting fraction below 100% (up to 10% if thin BP crystals were used). We estimate that only ~10  $\mu$ m thick surface layers were fully intercalated.

To determine a chemical composition of our intercalated compounds, we used energy dispersive X-ray spectroscopy (EDS). EDS typically probes a few-micron thick surface layer and is therefore the most appropriate method to determine the stoichiometry of our surface-intercalated samples. EDS spectra for our  $M_xP$  are shown in Fig. 1e and the corresponding elemental maps in Supplementary Figure S1. The distribution of intercalated metal atoms is fairly uniform for all  $M_xP$  compounds, and our EDS analysis yielded the average concentrations of 20 at.%, 17 at.%, 18 at.%, and 8 at.%, for K, Rb, Cs and Ca intercalated crystals, respectively (typical error in these measurements was 3 at %). Within this accuracy, the found concentrations correspond to the same composition of monovalent alkali-metal intercalated BP (namely,  $K_xP$ ,  $Rb_xP$ ,  $Cs_xP$  where  $x \approx 0.2$ ) and an approximately twice lower content for divalent Ca ( $Ca_xP$  with  $x \approx 0.1$ ). It was not possible to determine the concentration of Li using EDS because the technique is insensitive to elements with atomic numbers <5. The above compositions are stoichiometric (or stage-I, ref. <sup>29</sup>), in agreement with the first-principles calculations for Li, Na and Mg intercalation<sup>20,25,26</sup>, which predicted that the metal atoms should occupy certain positions between the puckered hexagonal layers, as shown in Fig. 1b.

We have also used X-ray diffraction (XRD) in order to probe the interlayer spacing after intercalation. For pristine black phosphorus our XRD spectra exhibited three main characteristic peaks at  $2\theta = 17.1^\circ$ ,  $34.4^\circ$  and  $52.5^\circ$ , corresponding to (020), (040) and (060) crystallographic planes, respectively (Supplementary Figure S2a). This gives a layer spacing of 5.18 Å, in agreement with other studies<sup>1,27</sup>. However, after intercalation, while the peaks characteristic of pristine BP have almost disappeared, as expected, no new peaks corresponding to an expanded crystal lattice are visible. We attribute this to the fact that intercalation is limited to ~10 $\mu$ m-thick layers near the surface, while X rays probe the entire volume of the crystals. Let us mention that such disappearance of XRD peaks is not unusual and was also reported for BP electrochemically intercalated with  $Na^+$  (ref. <sup>30</sup>). However, in contrast to the latter study, in our experiments the peaks corresponding to pristine BP re-appeared after exposure of the intercalated samples to air for about 100 hours (Supplementary Figure S2b) and all signs of superconductivity disappeared (Supplementary Figure S3). This indicates that, unlike the irreversible electrochemical intercalation<sup>12,30</sup>, our procedure preserved the original structure of the puckered BP layers.

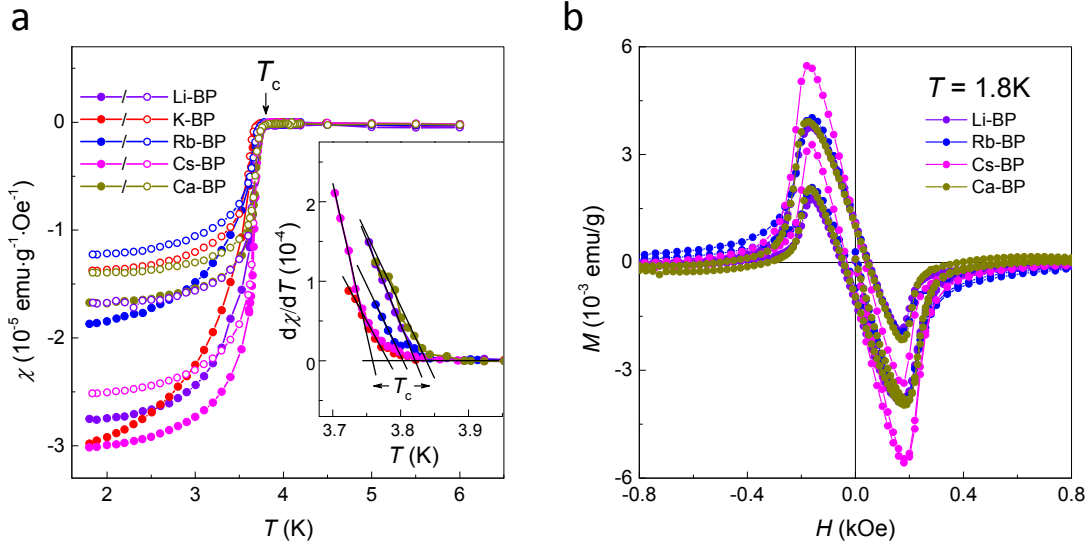


**Figure 2 | Superconductivity in intercalated black phosphorus. (a)** Temperature dependence of magnetic susceptibility  $\chi$  for Li, K, Rb, Cs and Ca intercalation. Shown are ZFC (solid symbols) and FC (open symbols) measurements for an in-plane magnetic field of 10 Oe. The arrow indicates  $T_c$  as determined from  $d\chi/dT$ . The inset shows how  $T_c$  was determined for individual samples: It is defined as the sharp change in  $d\chi/dT$  (see also Supplementary Fig. S4). **(b)** Magnetization  $M$  as a function of magnetic field for our intercalated compounds.

To detect the superconducting response, we used SQUID magnetometry (Methods). Figure 2a shows the temperature dependence of dc magnetic susceptibility  $\chi = M/H$  for all our intercalated BP compounds under zero-field-cooling (ZFC) and field-cooling (FC) conditions, and Fig. 2b provides examples of the magnetization as a function of applied magnetic field  $H$ . Here  $M$  is the magnetic moment. Both ZFC and FC curves show a sharp increase in diamagnetic susceptibility at 3.8 K, characteristic of a superconducting transition. To find the transition temperature, we used the derivatives of the ZFC curves, and  $T_c$  for each intercalated sample was determined as the temperature at which  $d\chi/dT$  exhibited a sharp increase (see inset in Fig. 2a and Supplementary Figure S4a). This yielded  $T_c = 3.8 \pm 0.1$  K for all  $M_xP$ , independent of the metal and whether it is monovalent or divalent. Note that we found no correlations between the observed slight variations in  $T_c$  and the intercalant (the same spread of  $\pm 0.1$  K in  $T_c$  was found for different samples intercalated with the same metal; Supplementary Fig. S4b).

To further characterize the superconductivity in our samples, we measured ac susceptibility,  $\chi_{ac}$ , as a function of both  $H$  and  $T$ . This allowed us to accurately determine the orientation-dependent critical field,  $H_c$ , corresponding to the disappearance of superconductivity, as shown in Fig. 3a, where the dc magnetization and ac susceptibility for a Cs-intercalated BP are shown together (more examples of ac susceptibility are shown in Supplementary Figure S5). These measurements were also used to find the temperature and orientation dependence of  $H_c$  as shown in Fig. 4. The  $H_c$  values were determined both from  $\chi_{ac}(H, T)$  (Fig. 3 and Supplementary Figure S5) and  $M(T, H)$  curves (Fig. 4a and Supplementary Figure S6), with good agreement between the values obtained by the two methods. Within our experimental accuracy, both parallel and perpendicular  $H_c(T)$  are universal for all  $M_xP$ , i.e. do not depend on the intercalant. This is similar to their intercalant-independent  $T_c$ .

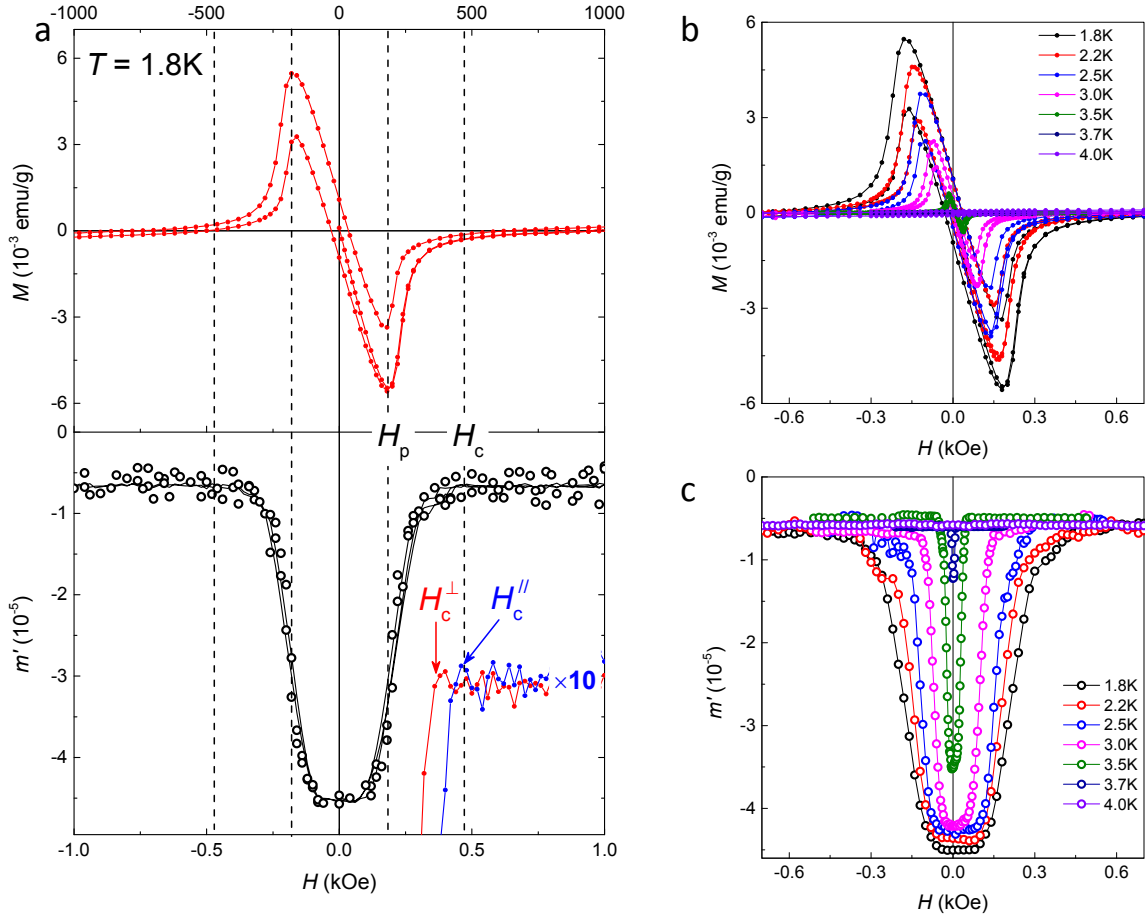


**Figure 3 | Magnetic field dependence of magnetization in  $M_xP$ .** (a) dc magnetization,  $M$ , and real part of ac susceptibility,  $m'$ , as a function of in-plane magnetic field,  $H$ . For clarity, only data for Cs-intercalated BP are shown. Open symbols are data points measured as the dc field varied from -1kOe to +1kOe and from +1kOe to -1kOe. Solid lines show the same data smoothed using Savitzky-Golay filter.  $H_p$  and  $H_c$  denote the penetration and critical magnetic field, respectively. Inset: Zoomed-up  $m'$  near the critical field in two orientations, with the arrows indicating  $H_c^\parallel$  and  $H_c^\perp$ . (b, c) Temperature dependences of  $M(H)$  and  $m'(H)$ . Only data for  $Cs_xBP$  are shown. Both types of measurements give the same values of  $T$ -dependent  $H_p$  and  $H_c$ .

Let us note that the superconducting fraction in the measurements shown in Figs. 2-4 was rather small,  $\sim 1\text{-}2\%$ , which we attribute to the dynamics of the intercalation process, as already mentioned above. It is much easier for metal ions to start intercalating between outer phosphorene layers, so that the process proceeds from the surface of each crystal into its bulk. The data in Figs. 2-4 were obtained on relatively large individual crystals,  $\sim 3 \times 2 \times 0.3$  mm, in order it would be possible to determine their orientation with respect to the applied magnetic field. By intercalating thinner crystals, with larger surface-to-volume ratios (Methods), we were able to increase the superconducting fraction to  $\sim 10\%$  (Supplementary Figure S7), which confirms the bulk nature of superconductivity.

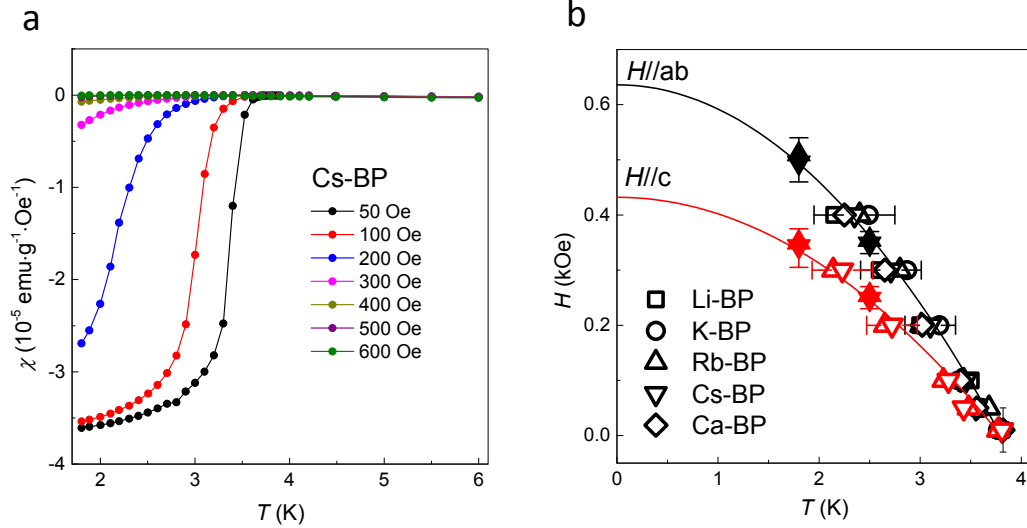


**Figure 4 | Transition temperature as a function of magnetic field. (a)** Temperature dependence of ZFC dc susceptibility  $\chi$  at different  $H$  applied parallel to the surface ( $ab$  plane). For clarity, only data for Cs-intercalated BP are shown. **(b)** Parallel and perpendicular critical fields as a function of temperature for all  $M_xP$  compounds in this study. Error bars indicate the accuracy of determination of the critical temperature from  $\chi(T)$  curves such as those shown in (a) (open symbols) and of the critical field from  $m'(H)$  (solid symbols). Solid curves are fits to the BSC expression  $H_c \propto 1 - (T/T_c)^2$ .

There are several notable features in the  $H$  dependence of intercalated BP's magnetization, both dc and ac (Figs. 2b and 3). Firstly, the  $M(H)$  curves are practically identical, apart from somewhat different absolute values of the maximum diamagnetic moment for different intercalating metals in Fig. 2b, which is related to different superconducting fractions. Indeed, all the compounds exhibit the same penetration field,  $H_p$  (1.8 K)  $\sim$  180 Oe (determined from dc magnetization curves as shown in Fig. 3a), and the same magnetic field corresponding to the disappearance of the diamagnetic response,  $H_c$  (1.8 K)  $\sim$  500 Oe. Secondly, the sharp fall in  $M$  just above  $H_p$  is reminiscent of the behaviour of type-I, rather than type II, superconductors. In the former case, the magnetic field penetrates either uniformly at the thermodynamic critical field,  $H_m$ , destroying superconductivity or, for a finite demagnetization factor, in the form of normal domains<sup>31</sup>. The relatively rapid decrease is also seen in ac susceptibility (Fig. 3). However, there is a clear difference from a typical type I superconductor with the Ginzburg-Landau parameter  $\kappa \ll 1$  if we compare our  $M(H)$  curves in Fig. 2 with  $M(H)$  for indium that we used as a reference (Supplementary Figure S8). The 'tail' on the  $M$  and  $m'$  curves seen at  $H > 300$  Oe corresponds to small but still finite diamagnetic response above  $H_p$ . This behaviour suggests that the intercalated BP is probably a borderline type I/type II superconductor with  $\kappa$  close to the critical value of  $\approx 0.7$ , similar to Nb (ref.<sup>32</sup>). Thirdly and very unusually, the  $M(H)$  curves for all  $M_xP$  compounds display practically the same hysteresis (trapping of the magnetic flux). The latter corresponds to pinning of the magnetic flux by defects or impurities<sup>31</sup> and, therefore, is sensitive not only to a particular chemical compound, but also to structural details of individual samples. The fact that, in our case, different intercalated compounds trap the same amount of flux at  $H = 0$  also points in the direction of type-I superconductivity because pinning of superconducting domains is known to be less sensitive to crystal imperfections<sup>31,33</sup>.

To relate the appearance of superconductivity with the structural changes in BP which occur as a result of intercalation, we used Raman spectroscopy (Supplementary Figure S9). The well-known

signatures of phonon modes in BP (ref.<sup>30,34</sup>) could be compared before and after intercalation. Raman spectroscopy is sensitive to the properties of a few near-surface layers and, therefore, probes the same part of the crystals as EDS and magnetization measurements. Atomic displacements corresponding to the Raman modes are illustrated in Supplementary Figure S9a. There are three main phonon modes that in our pristine BP result in peaks at 362, 440 and 467  $\text{cm}^{-1}$  (see Supplementary Figure S9b). From comparison of the Raman spectra for pristine and intercalated BP it is clear that intercalation has only a small effect on atomic vibrations of P atoms. The modes are slightly broadened but essentially unchanged, which is consistent with the preserved structure of phosphorene layers and in agreement with the mentioned experiments in which samples exposed to air recovered their initial structural state. At the same time, one can see a clear shift of all three modes to lower frequencies, corresponding to phonon softening within phosphorene layers. Such softening is expected as a result of the doping of phosphorene, which according to the first-principle calculations<sup>19,20</sup> should result in charge transfer of  $0.8e^-$  per P atom for monovalent and  $1.5e^-$  for divalent donors.

The most surprising result of our work is the practically identical superconducting characteristics of all the tested intercalated compounds, independent of the mass and atomic radius of the intercalating metal and its valency, i.e. the lack of any isotope-like effect. This is in stark contrast to other superconducting intercalated compounds, of which intercalated graphite is an archetypal example and has obvious structural similarities with BP. In the case of intercalated graphite, its superconducting properties are strongly dependent on the chemical composition, with the critical temperature ranging from 0.02 K for Cs-intercalated graphite to 11.5 K for  $\text{CaC}_6$  (ref.<sup>35</sup>) and  $\text{LiC}_6$  not superconducting at all. The mechanism of superconductivity in the intercalated graphite compounds is well understood<sup>36,37,38</sup>. In terms of the standard phonon-mediated superconductivity, superconductivity in graphite cannot be achieved within individual electron-doped graphene layers because the frequencies of in-plane graphene phonons are too high to lead to efficient electron-phonon coupling, whereas the planar structure of graphene forbids coupling between the  $\pi^*$  electronic states and softer out-of-plane vibrations<sup>36</sup>. Therefore, an incomplete ionization and a partially occupied metal-derived electronic band is a key for achieving superconductivity in intercalated graphite<sup>36,37</sup>, and the superconductivity cannot be attributed to either the graphene  $\pi^*$  band or the metal-derived electronic band alone. Instead, the interaction between these two bands plays a critical role, according to theory, and the transition temperature is strongly dopant dependent.

The situation in black phosphorus is quite different. The experiment clearly shows that the chemical composition of intercalated BP is irrelevant for the occurrence of superconductivity, and one has to find a physical mechanism relying on heavy electron doping of individual phosphorene layers. This is in good agreement with theoretical expectations. Indeed, the puckered structure and  $sp^3$  hybridization of phosphorene layers remove the symmetry constraints on electron-phonon coupling<sup>20</sup>, with more phonon modes able to contribute, increasing the overall coupling constant,  $\lambda$ . In addition, electron transfer from intercalant atoms to phosphorene softens its vibrational modes, especially the sublayer breathing modes, further enhancing  $\lambda$  without the need of changing the crystal symmetry of phosphorene layers<sup>19,20</sup>. In our experiments such phonon softening is clear from the Raman spectra, where a similar frequency shift is observed for all intercalants (Supplementary Figure S9b). Furthermore, recent calculations for Li-intercalated bilayer phosphorene<sup>20</sup> indicate that

the electronic bands near the Fermi level of intercalated BP are mainly  $\pi^*$ -like bands derived from phosphorene, while the contribution to the density of states from the metal-derived band is very small. This basically means that the superconductivity is intrinsic to individual phosphorene layers rather than the entire compound, in agreement with our experiments. Let us mention that the theoretical explanation is also consistent with recent ARPES measurements of the BP intercalated with K (ref. <sup>18</sup>) or Li (ref. <sup>39</sup>), which found no additional interlayer bands that could be attributed to the alkali metals.

The intercalant-independent  $T_c$  implies the same doping level induced within phosphorene layers. The situation is somewhat similar to equal doping and intercalant-independent  $T_c$  in K, Rb and Cs-intercalated  $\text{MoS}_2$  (refs. 40,41). This is also in agreement with theory. The first-principle calculations<sup>25</sup> found an optimum charge transfer for monovalent alkali atoms (Li and Na) of  $0.8 e^-$  per P atom and for divalent Mg of  $1.5 e^-$ . It is reasonable to expect the same electron doping for K, Rb and Cs that were not covered in the calculations and a close doping for divalent Ca that is chemically similar to Mg and intercalates in twice smaller concentrations than alkali metals. Furthermore, several studies, both theoretical<sup>25</sup> and experimental<sup>12</sup> found that the stoichiometric composition  $\text{M}_{0.2}\text{P}$  found in our studies is the maximum – and probably optimum – alkali content, for which the structure of phosphorene layers is preserved and the intercalation can be reversed. If more metal atoms are forced into the space between phosphorene layers by, e.g., electrochemical intercalation<sup>12,30</sup>, this leads to irreversible changes including chemical bonding and formation of new alloys. Taken together, the available evidence suggests that the amount of intercalating metal atoms in BP is determined primarily by an electrostatic-like equilibrium between the charged phosphorene layers and metal ions. In our case, this conclusion is supported by the factor-of-2 difference in the concentration of monovalent and divalent intercalants as found experimentally.

In summary, we have achieved successful intercalation of black phosphorus with several alkali and alkali-earth metals using the liquid ammonia method. The intercalated compounds exhibit universal superconducting properties: same  $T_c = 3.8 \pm 0.1 \text{ K}$ , same critical fields  $H_c^{\parallel}(0) \sim 630 \text{ Oe}$  and  $H_c^{\perp}(0) \sim 440 \text{ Oe}$  and even similar flux pinning. The lack of variations strongly suggests a physical mechanism behind the superconductivity, such as doping of phosphorene layers by intercalating atoms. In this respect, intercalated BP is very different from extensively-studied intercalated graphite compounds, despite their structural similarities. In the latter case, both electronic and phonon contributions from intercalated metal layers play a key role in inducing superconductivity. In intercalated BP, the superconductivity can entirely be attributed to electron-doped phosphorene whereas changes in the electron and phonon spectra induced by intercalation play little role, according to the experiment and in qualitative agreement with theory. Nevertheless, the degree to which the superconducting behavior disregards the chemical composition is puzzling and perhaps suggests some more fundamental rules at play behind the observed superconductivity.

## Methods

To achieve intercalation, BP crystals (99.998%, Smart Elements) and a desired metal (99.95% Li, K, Rb, Cs and Ca from Aldrich) were sealed in a quartz tube under the inert atmosphere of a glove box with oxygen and moisture levels less than 0.5 ppm. The reactor tube was then evacuated to  $\approx 10^{-5}$  mbar, connected to a cylinder of pressurised ammonia (99.98% from CK Gas) and placed in a bath of dry-



ice/ethanol (-78 °C). As gaseous ammonia was allowed into the reactor tube, it condensed onto the reactants (BP and the metal), dissolving the metal and forming a deep-blue solution. The colour depth was used as an indicator of the concentration of dissolved metal<sup>28</sup>. To prevent contamination with oxygen or moisture, the empty space in the reactor tube left after ammonia condensation was filled with argon gas (Zero-Grade from BOC). The tube was kept in the dry-ice/ethanol bath for 48 h, after which the system was warmed up, ammonia and argon evacuated and the intercalated BP recovered inside the glove box. As alkali-metal intercalated compounds are extremely sensitive to oxygen and moisture, they were handled in the inert atmosphere of the glovebox, immersed in paraffin oil or protected by using sealed containers. As a reference, we tested our method by intercalating MoS<sub>2</sub> with different alkalis, which produced superconducting samples with  $T_c \approx 6.9$  K, in agreement with literature<sup>41</sup>. In addition, to ensure that the observed superconductivity could not be related to accidental contamination, we used mixtures of BP and alkali metals (without placing them in liquid ammonia) and measured their magnetization. No superconducting response could be detected unless the intercalation reaction was induced.

The chemical composition was determined using EDS (Oxford Instruments X-Max detector integrated with Zeiss' Ultra scanning electron microscope). The metal content was determined at 10 or more randomly selected areas on each sample and the average was taken as the intercalant concentration.

X-ray powder diffraction (XRD) measurements were performed using Bruker D8 Discover diffractometer with Cu K $\alpha$  radiation ( $\lambda = 1.5406$  Å). Before each measurement, samples were roughly ground and mixed with paraffin oil, and then sealed in an airtight XRD sample holder (Bruker, A100B36/B37) inside the glove-box. XRD spectra were obtained at room temperature in the 2 $\theta$  range of 5–75° with a step of 0.03° and a dwell time of 0.5 s/step.

Raman spectroscopy was performed at room temperature using the Renishaw inVia Reflex system with a 532-nm laser. All spectra were recorded using a power of ~1 mW with the samples sealed between two thin glass plates.

Magnetization measurements were carried out using Quantum Design MPMS-XL7 SQUID magnetometer. To protect the intercalated samples from degradation they were immersed in paraffin oil and sealed inside polycarbonate capsules in a dry argon atmosphere of the glovebox. Measurements were carried out in a dc magnetic field applied either parallel or perpendicular to the crystal surface. Temperature dependences were measured in zero-field cooling and field-cooling modes. In the former, the samples were cooled in zero magnetic field from ~10 to 1.8 K, then the field  $H$  was applied and  $M$  was measured as the temperature increased from 1.8 to, typically, 6 K. In latter mode,  $M(T)$  was measured as the temperature decreased from above 6 to 1.8 K. The ac susceptibility was measured using ac magnetic fields (typically, 1 Oe at 8 Hz) applied parallel to the dc field.

To estimate the superconducting fraction in different samples, we used the initial (Meissner) slope of the  $M(H)$  curves (for a 100% superconducting sample the slope should be  $-1/4\pi$ ). This yielded a fraction of ~1-2% if relatively large (~3×2×0.3 mm) crystals were intercalated. To increase the intercalated volume, we used two different methods. First, a crystal of BP was ground into a powder consisting of many smaller platelet-shaped crystals that were then intercalated as described above.

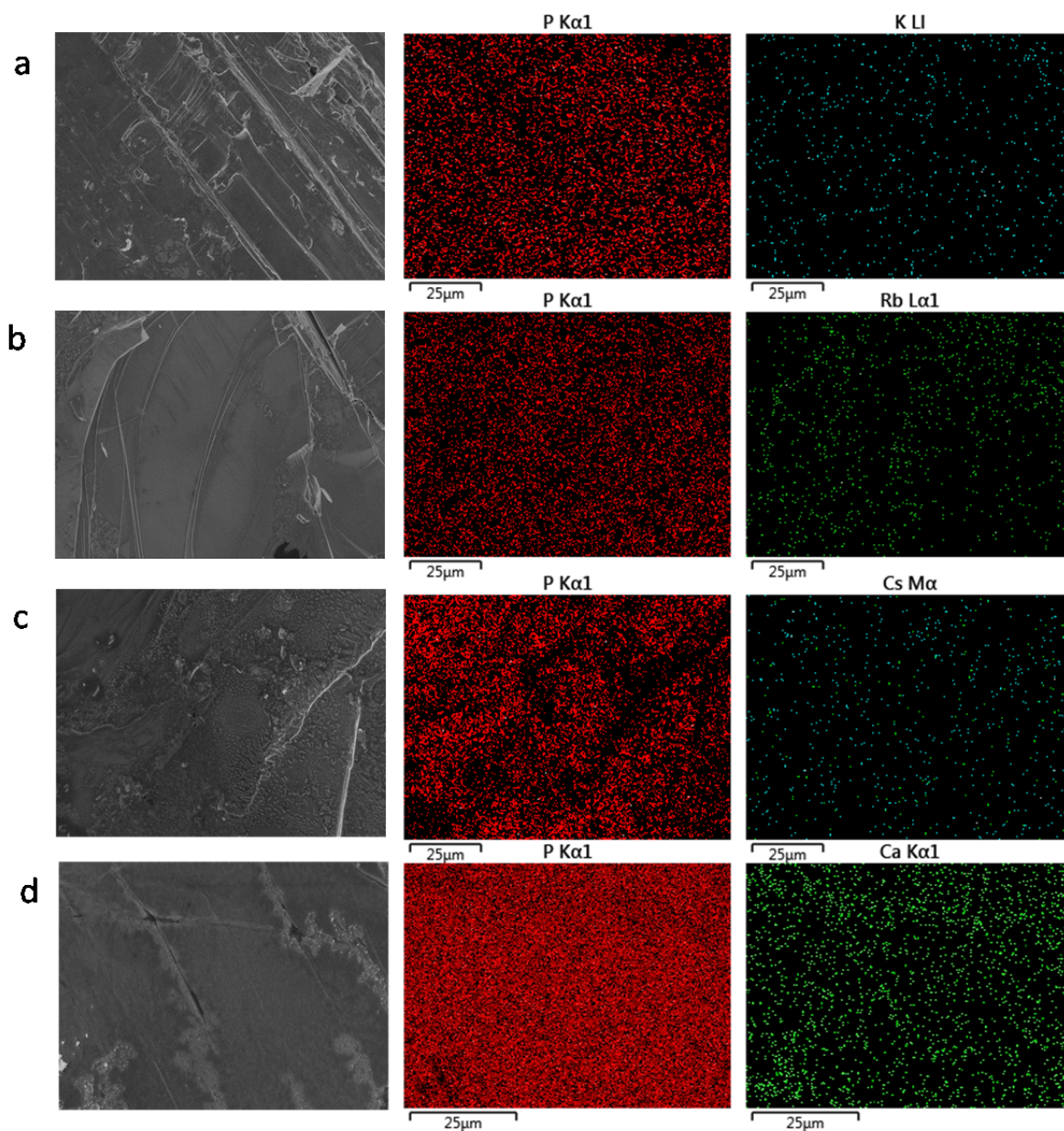
This increased the superconducting fraction by a factor of  $\sim 3$ . However, we believe that the smallest BP crystals within this powder were non-superconducting, reacting with minute amounts of oxygen and moisture left even under inert atmosphere<sup>3</sup>. The second and more successful approach was to break up BP crystals into smaller ones during the intercalation process. To this end, the liquid ammonia solution was subjected to mild shaking using a magnetic stirrer. This allowed an increase in the superconducting fraction to  $\sim 10\%$ .

## References

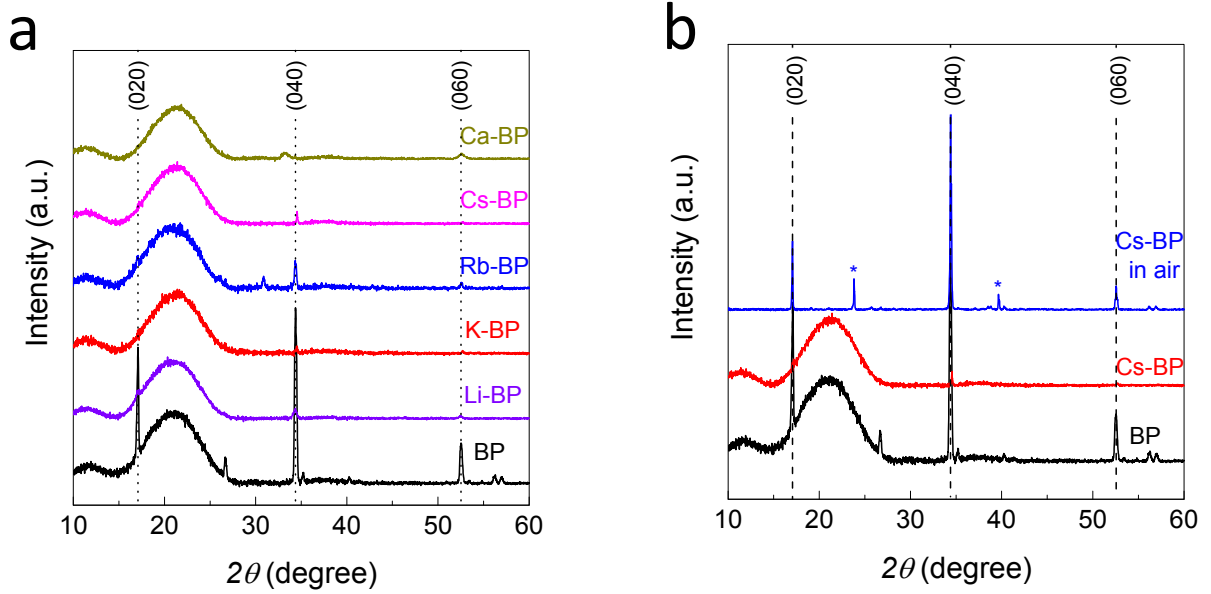
- 1 Ling, X., Wang, H., Huang, S., Xia, F. & Dresselhaus, M. S. The renaissance of black phosphorus. *Proc. Natl. Acad. Sci. USA* **112**, 4523-4530 (2015).
- 2 Liang, L. *et al.* Electronic bandgap and edge reconstruction in phosphorene materials. *Nano lett.* **14**, 6400-6406 (2014).
- 3 Cao, Y. *et al.* Quality heterostructures from two-dimensional crystals unstable in air by their assembly in inert atmosphere. *Nano lett.* **15**, 4914-4921 (2015).
- 4 Li, L. *et al.* Quantum oscillations in a two-dimensional electron gas in black phosphorus thin films. *Nat. Nanotechnol.* **10**, 608-613 (2015).
- 5 Low, T. *et al.* Tunable optical properties of multilayer black phosphorus thin films. *Phys. Rev. B* **90**, 075434 (2014).
- 6 Wittig, J. & Matthias, B. Superconducting phosphorus. *Science* **160**, 994-995 (1968).
- 7 Karuzawa, M., Ishizuka, M. & Endo, S. The pressure effect on the superconducting transition temperature of black phosphorus. *J. Phys. Condens. Matter* **14**, 10759 (2002).
- 8 Jamieson, J. C. Crystal structures adopted by black phosphorus at high pressures. *Science* **139**, 1291-1292 (1963).
- 9 Maruyama, Y. *et al.* Electronic properties of black phosphorus single crystals and intercalation compounds. *Bull. Chem. Soc. Jpn.* **59**, 1067-1071 (1986).
- 10 Nishii, T., Maruyama, Y., Inabe, T. & Shirotni, I. Synthesis and characterization of black phosphorus intercalation compounds. *Synth. Met.* **18**, 559-564 (1987).
- 11 Maruyama, Y., Suzuki, S., Kobayashi, K. & Tanuma, S. Synthesis and some properties of black phosphorus single crystals. *Phys. B+ C* **105**, 99-102 (1981).
- 12 Xia, W. *et al.* Visualizing the electrochemical lithiation/delithiation behaviors of black phosphorus by in situ transmission electron microscopy. *J. Phys. Chem. C* **120**, 5861-5868 (2016).
- 13 Bridgman, P. Two new modifications of phosphorus. *J. Am. Chem. Soc.* **36**, 1344-1363 (1914).
- 14 Keyes, R. W. The electrical properties of black phosphorus. *Phys. Rev.* **92**, 580 (1953).
- 15 Li, L. *et al.* Black phosphorus field-effect transistors. *Nat. Nanotechnol.* **9**, 372-377 (2014).
- 16 Rodin, A., Carvalho, A. & Neto, A. C. Strain-induced gap modification in black phosphorus. *Phys. Rev. Lett.* **112**, 176801 (2014).
- 17 Li, Y., Yang, S., Li, J. Modulation of the Electronic Properties of Ultrathin Black Phosphorus by Strain and Electrical Field. *J. Phys. Chem. C* **118**, 23970-23976 (2014)
- 18 Kim, J. *et al.* Observation of tunable band gap and anisotropic Dirac semimetal state in black phosphorus. *Science* **349**, 723-726 (2015).
- 19 Shao, D., Lu, W., Lv, H. & Sun, Y. Electron-doped phosphorene: a potential monolayer superconductor. *EPL* **108**, 67004 (2014).
- 20 Huang, G., Xing, Z. & Xing, D. Prediction of superconductivity in Li-intercalated bilayer phosphorene. *Appl. Phys. Lett.* **106**, 113107 (2015).
- 21 Saito, Y. & Iwasa, Y. Ambipolar insulator-to-metal transition in black phosphorus by ionic-liquid gating. *ACS Nano* **9**, 3192-3198 (2015).

- 22 Ye, J. *et al.* Superconducting dome in a gate-tuned band insulator. *Science* **338**, 1193-1196 (2012).
- 23 Zhang, R. *et al.* Superconductivity in potassium-doped metallic polymorphs of MoS<sub>2</sub>. *Nano Lett.* **16**, 629-636 (2015).
- 24 Friend, R. & Yoffe, A. Electronic properties of intercalation complexes of the transition metal dichalcogenides. *Adv. Phys.* **36**, 1-94 (1987).
- 25 Hembram, K. P. *et al.* A comparative first-principles study of the lithiation, sodiation, and magnesiation of black phosphorus for Li-, Na-, and Mg-ion batteries. *Phys. Chem. Chem. Phys.* **18**, 21391-21397 (2016).
- 26 Hembram, K. *et al.* Unraveling the atomistic sodiation mechanism of black phosphorus for sodium ion batteries by first-principles calculations. *J. Phys. Chem. C* **119**, 15041-15046 (2015).
- 27 Brown, A. & Rundqvist, S. Refinement of the crystal structure of black phosphorus. *Acta Crystallogr.* **19**, 684-685 (1965).
- 28 Catterall, R. & Mott, N. Metal-ammonia solutions. *Adv. Phys.* **18**, 665-680 (1969).
- 29 Dresselhaus, M.S. & Dresselhaus, G. Intercalation compounds of graphite. *Adv. Phys.* **51**, 1-186 (2002)
- 30 Sun, J. *et al.* A phosphorene–graphene hybrid material as a high-capacity anode for sodium-ion batteries. *Nat. Nanotechnol.* **10**, 980-985 (2015).
- 31 Poole, C. K., Farach, H. A. & Creswick, R. J. *Handbook of Superconductivity*. (Academic Press, 1999).
- 32 Finnemore, D., Stromberg, T. & Swenson, C. Superconducting properties of high-purity niobium. *Phys. Rev.* **149**, 231 (1966).
- 33 Provost, J., Paumier, E. & Fortini, A. Shape effects on the magnetization of superconducting lead at 4.2 K. *J. Phys. F: Metal Phys.* **4**, 439 (1974).
- 34 Sugai, S. & Shirotani, I. Raman and infrared reflection spectroscopy in black phosphorus. *Solid State Commun.* **53**, 753-755 (1985).
- 35 Weller, T. E., Ellerby, M., Saxena, S. S., Smith, R. P. & Skipper, N. T. Superconductivity in the intercalated graphite compounds C<sub>6</sub>Yb and C<sub>6</sub>Ca. *Nature Phys.* **1**, 39-41 (2005).
- 36 Profeta, G., Calandra, M. & Mauri, F. Phonon-mediated superconductivity in graphene by lithium deposition. *Nature Phys.* **8**, 131-134 (2012).
- 37 Mazin, I. Intercalant-driven superconductivity in YbC<sub>6</sub> and CaC<sub>6</sub>. *Phys. Rev. Lett.* **95**, 227001 (2005).
- 38 Chapman, J. *et al.* Superconductivity in Ca-doped graphene laminates. *Sci. Rep.* **6**, 23254 (2016).
- 39 Sanna, A. *et al.* First-principles and angle-resolved photoemission study of lithium doped metallic black phosphorous. *2D Materials* **3**, 025031 (2016).
- 40 R. B. Somoano, V. Hadek, and A. Rembaum. Alkali metal intercalates of molybdenum disulfide. *J. Chem. Phys.* **58**, 697-701 (1973).
- 41 J. A. Woollam and R. B. Somoano. Physics and chemistry of MoS<sub>2</sub> intercalation compounds. *Mater. Sci. Eng.* **31**, 289-295 (1977).

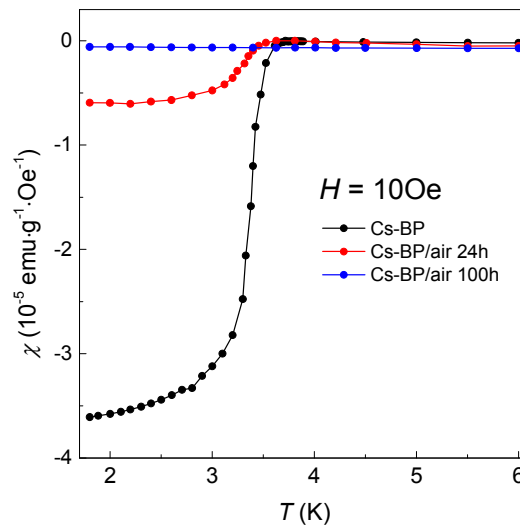
## SUPPLEMENTARY INFORMATION



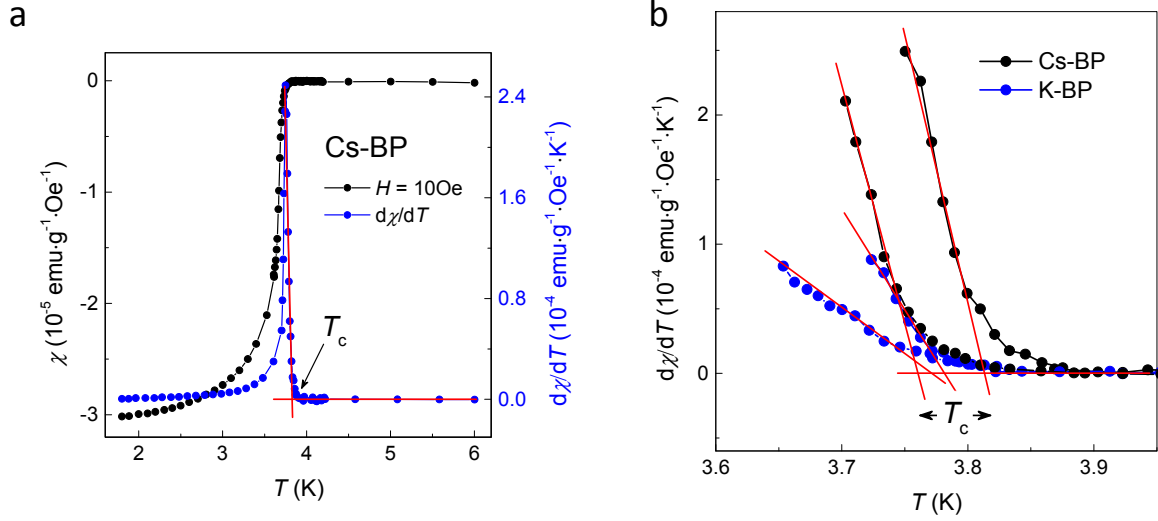
**Supplementary Figure S1 | Distribution of metal dopants in intercalated black phosphorus from EDS analysis. (a-d)** Shown are SEM images (left column) and corresponding elemental maps for K-, Rb-, Cs- and Ca-intercalated black phosphorus, respectively. For all intercalated samples, the distribution of intercalants follows closely the shape of the crystals as seen from the distribution of P atoms.



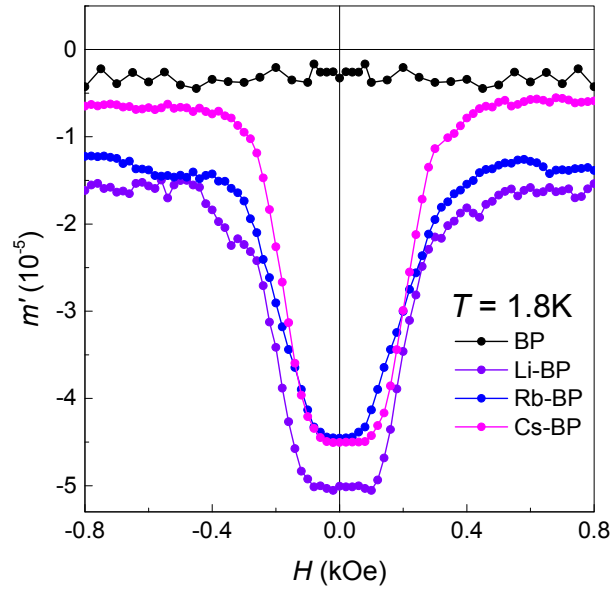
**Supplementary Figure S2 | X-ray diffraction spectra for pristine, intercalated and de-intercalated black phosphorus.** (a) XRD spectra for pristine and intercalated BP. Dashed lines indicate known positions of (020), (040) and (060) peaks for pristine BP. (b) Comparison of XRD spectra for pristine BP (black curve), Cs-intercalated BP (red curve) and the same Cs-intercalated sample that was allowed to de-intercalate by exposure to air for 100 hours (blue curve). \* indicates the known peaks for Cs hydroxide.



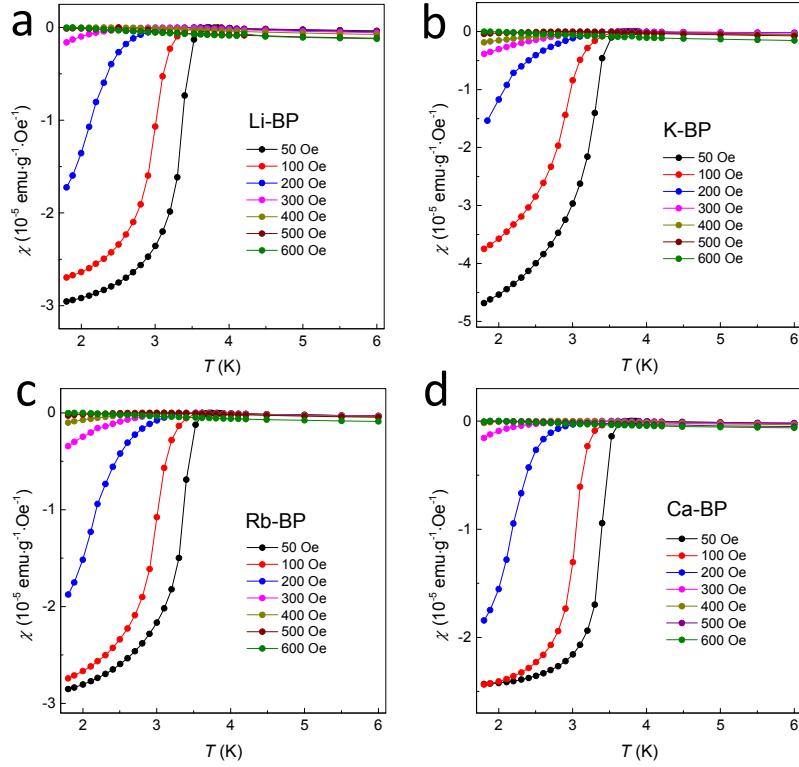
**Supplementary Figure S3 | Air sensitivity and de-intercalation of superconducting black phosphorus.** Shown is ZFC magnetic susceptibility,  $\chi(T)$ , of a Cs-intercalated BP sample before (black symbols) and after exposure to air for 24 hours (red symbols) and for 100 hours (blue symbols).



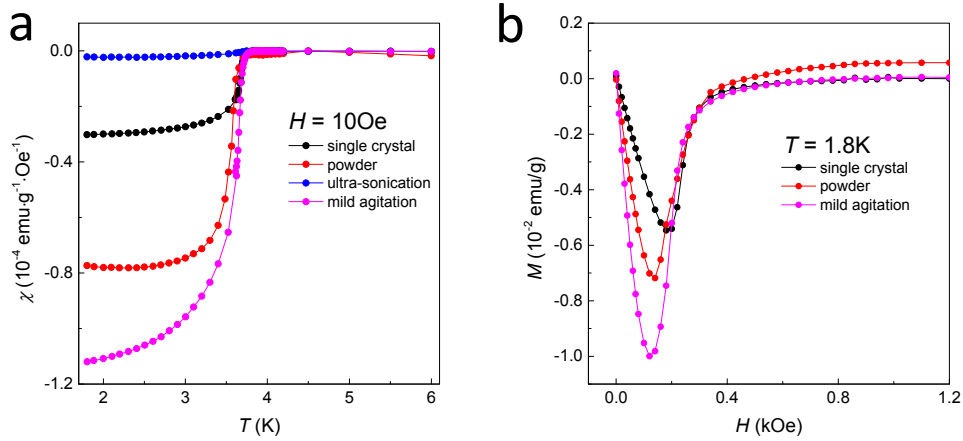
**Supplementary Figure S4 | Determination of the critical temperature  $T_c$ .** (a) ZFC magnetic susceptibility,  $\chi(T)$ , for Cs-intercalated BP (black symbols). Blue symbols show the corresponding numerical derivative  $d\chi/dT$ .  $T_c$  is determined as the temperature corresponding to a sharp increase in  $d\chi/dT$  and is given by a crossing point of the linear extrapolations of the corresponding parts of the curve. (b) Examples of  $T_c$ 's for different samples intercalated with the same metal. The spread of  $T_c$ 's for the same intercalant is similar to that for different intercalating metals (cf. inset in Fig. 2a in the main text) and limits our accuracy in finding the exact  $T_c$ .



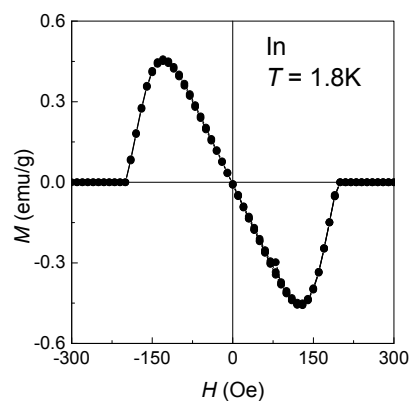
**Supplementary Figure S5 | Magnetic-field dependent ac susceptibility of Li, Rb and Cs intercalated BP.** Shown is real part of ac susceptibility,  $m'$ , versus  $H$  at  $T = 1.8 \text{ K}$ .



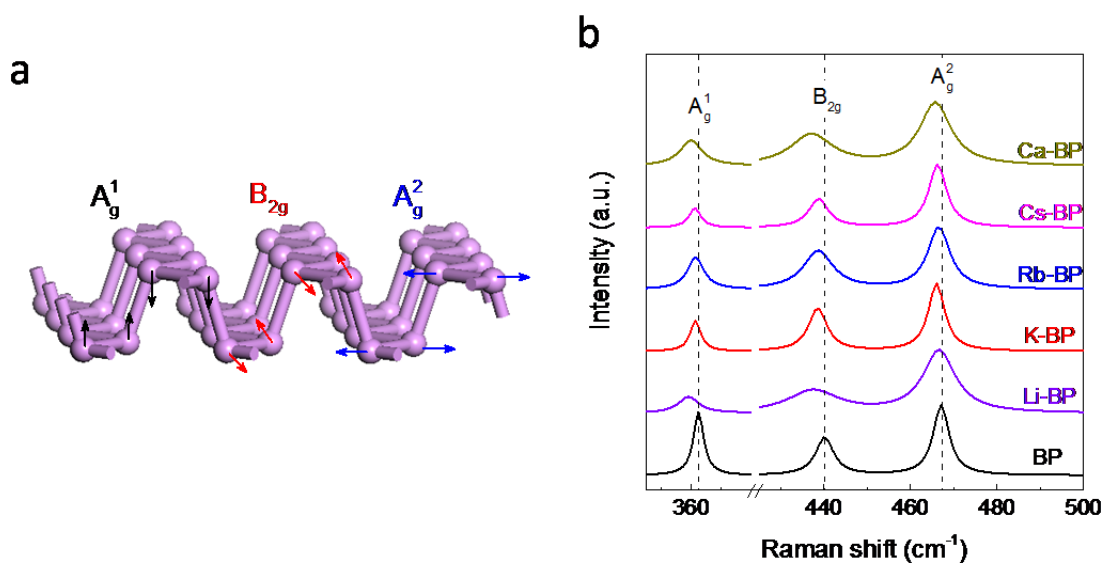
**Supplementary Figure S6 | Suppression of superconductivity by magnetic field in intercalated BP.** (a-d) ZFC dc susceptibility,  $\chi = M/H$ , as a function of temperature at different magnetic fields,  $H$ , for Li-, K-, Rb- and Ca-intercalated BP, respectively.



**Supplementary Figure S7 | Increasing the superconducting fraction in intercalated BP.** Field-dependent magnetization,  $M(H)$ , and temperature-dependent dc susceptibility,  $\chi(T)$ , for BP intercalated with Cs under different conditions (see Methods for details). Black symbols correspond to the magnetic response of a large,  $\sim 3 \times 5 \times 0.3 \text{ mm}$  BP crystal intercalated with Cs. Red symbols correspond to intercalation of BP powder (a large crystal ground into powder prior to intercalation). Magenta and blue symbols correspond to the superconducting response of a large crystal that was broken up into many smaller and thinner crystals during intercalation by subjecting the liquid-ammonia solution to mild agitation and ultra-sonication, respectively. While mild agitation led to an increase of the superconducting fraction to  $\sim 10\%$ , ultra-sonication resulted in suppression of superconductivity, presumably due to excessive damage to the BP crystal.



**Supplementary Figure S8 | Magnetic-field dependent magnetization of a typical type-I superconductor.** Shown is dc magnetization,  $M$ , as a function of magnetic field,  $H$ , at  $T = 1.8$  K for an indium (In) sample. The curves measured from -300 to 300 Oe and from 300 to -300 Oe overlap, due to the absence of flux pinning.



**Supplementary Figure S9 | Raman spectra for pristine and intercalated black phosphorus. (a)** Schematic representation of the atomic displacements corresponding to Raman-active modes in BP. **(b)** Raman spectra for pristine and metal-intercalated black phosphorus (see labels). Dashed lines indicate the positions of the  $A_g^1$ ,  $B_{2g}$  and  $A_g^2$  Raman peaks for pristine BP.